Nanoscience and Nanotechnology Letters
Vol. 7, 387–391, 2015

Special *P–N* Junction Photocatalytic NiO/Ag_2S Nanocomposite Synthesized by Hydrothermal Method

Ruiqiang Ding[1], Han Dai[1], Meicheng Li[1,2,*], Bing Jiang[1], MwenyaTrevora[1], Dandan Song[1], and Chao Geng[2]

[1]*State Key Laboratory of Alternate Electrical Power System with Renewable Energy Sources, School of Renewable Energy, North China Electric Power University, Beijing 102206, China*
[2]*Chongqing Materials Research Institute, Chongqing 400707, China*

A special photocatalytic NiO/Ag_2S nanocomposite is synthesized by hydrothermal method. Combined the photocatalytic properties of both NiO and Ag_2S, the NiO/Ag_2S nanocomposite shows high photocatalytic properties in methylene orange degeneration tests. Through the experiment analysis, the high photocatalytic properties of NiO/Ag_2S nanocomposite are attributed to the uniform mixing of these two materials and the induced *n–p* junction at the interfacial contact between the NiO and Ag_2S phases. This work offers novel NiO/Ag_2S nanocomposites which have great potential applications in visible light photocatalysis.

Keywords: Nanocomposite, Hydrothermal Method, *p–n* Junction, Morphology, Photocatalytic.

1. INTRODUCTION

In recent decades, the nanocomposites with two or more different functional materials have been investigated across vast fields for their unique physicochemical functionalities. As one of the most important *n*-type semiconductor materials, Ag_2S nanoparticles with narrow-band-gap (3.55 eV) and excellent visible light absorption properties have attracted great research interests in photoelectric, medical devices, and photocatalysis.[1–3] However, the serious agglomeration and the recombination of photo-generated electron–holes of the Ag_2S nanoparticles still limit their applications. Some pioneer works show that these problems would be partial resolved by combining Ag_2S nanoparticles with other materials (metal or compound) into nanocomposites, such as Ag_2S–Ag, Ag_2S–Au, Ag_2S–ZnO, Ag_2S–TiO_2, Ag_2S–SnO etc.[4–8] These nanocomposites usually exhibit better physicochemical properties than those of each individual material.

Recently, a promising approach of establishing *p–n* junction at the interfacial contact has been proposed as an effective way to prevent the electron–hole pair recombination and prolong the electron's lifetime.[9,10] As a *p*-type wide-band-gap (3.55 eV) semiconductor, nickel oxide (NiO), has received much attention owing to its low cost, possessing unique catalytic,[11,12] special electric and magnetic properties.[13–15] The characteristics of *p–n* junction structures can be used to remedy the disadvantages of Ag_2S nanoparticles in photocatalysis.[16–20]

In this work, a novel NiO/Ag_2S nanocomposite is successfully synthesized by a facile hydrothermal process. Through the analysis of morphology of the NiO/Ag_2S nanocomposite, it was found that NiO flower shaped structures are favorable to combine with Ag_2S nanoparticles to form NiO/Ag_2S nanocomposite. Methylene orange was used to test the photocatalytic ability of the nanocomposite. Compared with the physical mixtures of NiO and Ag_2S, the novel nanocomposites show better photocatalytic properties. The mechanism of the photocatalytic enhancement of the NiO/Ag_2S nanocomposites is also analyzed in this work.

2. EXPERIMENTAL DETAILS

2.1. Materials

Nickel chloride, polyethylene glycol 400, sodium acetate, silver nitrate, sodium sulfide were used for the synthesis of NiO/Ag_2S nanocompsites. All chemicals were in analytical grade and used without further purification. Methyl Orange (MO) dye was employed as a model wastewater contaminant for the photocatalytic activity tests in work.

*Author to whom correspondence should be addressed.

 1941-4900/2015/7/387/005 doi:10.1166/nnl.2015.1978

2.2. Synthesis Procedure

The NiO nanostructures were firstly synthesized by a hydrothermal and calcination process. A specified amount of nickel chloride (0.25 g), polyethylene glycol 400 (0.2 g), sodium acetate (0.5 g) were dissolved in the 40 mL mixed solution of ethylene glycol and deionized water (volume ratio is 1:1) and stirred vigorously until to clear. The solution was placed in a 50 mL teflon-lined stainless autoclave, and then heated to 140 °C and remained for 10 h under autogenous pressure. Afterwards, green nickelous hydroxide suspensions were obtained after the autoclave was cooled down to room temperature. Then the suspensions were centrifuged at 7000 r/min for 5 min. The liquid was then taken from the centrifugal tube with the sediment retained, followed by dropwise adding anhydrous ethanol into the centrifugal tube and centrifuged again under the same condition. The green sediment was harvested by vacuum drying at 80 °C for 10 h. The green powder was obtained after drying and annealing at 400 °C in air for 2 h. The gray NiO nanoparticle powder was harvested and washed three times with absolute ethyl alcohol to remove chloridion and vacuum drying at 80 °C for 5 h. Thereafter, 0.2 g of NiO was joined in 30 mL deionized water with magnetic stirring. Then sodium sulfide solution (20 mL) was added dropwise into the above solution with stirring at room temperature for 1 h. The mixture solution was placed in a 50 mL teflon-lined stainless autoclave, and heated to 150 °C for 10 h under autogenous pressure. After cooling down to room temperature, the black turbid liquid was centrifuged and washed twice with anhydrous ethanol, and then dried under vacuum at 80 °C for 5 h. Finally, the black powder of NiO/Ag_2S nanocomposites was obtained.

2.3. Characterization Techniques

Morphology, structure and component were investigated by scanning electron microscope (SEM, FEI Quanta200F), transmission electron microscopy and energy-dispersive X-ray spectroscopy (EDX, JEOL JEM-2100). The X-ray diffraction (XRD) technique was used to identify the crystalline phases of the samples. Arotating anode XRD system (Rigaku, PMG-A2) generating monochromated Cu-Ka radiation was employed to obtain XRD patterns by using a continuous scanning mode at a rate of 5 degree/min under operating conditions of 35 kV and 15 mA. An UV-visible spectrophotometer (Shimadzu, UV-2600) was used to record absorbance spectra of the samples at room temperature with $BaSO_4$ as the reference. The photocatalytic reduction of methyl orange (MO) in aqueous solution was also studied under 500 W Xe lamp irradiation.

3. RESULTS AND DISCUSSION

The surface morphologies of NiO nanostructures, Ag_2S nanoparticles, physical mixtures of NiO and Ag_2S,

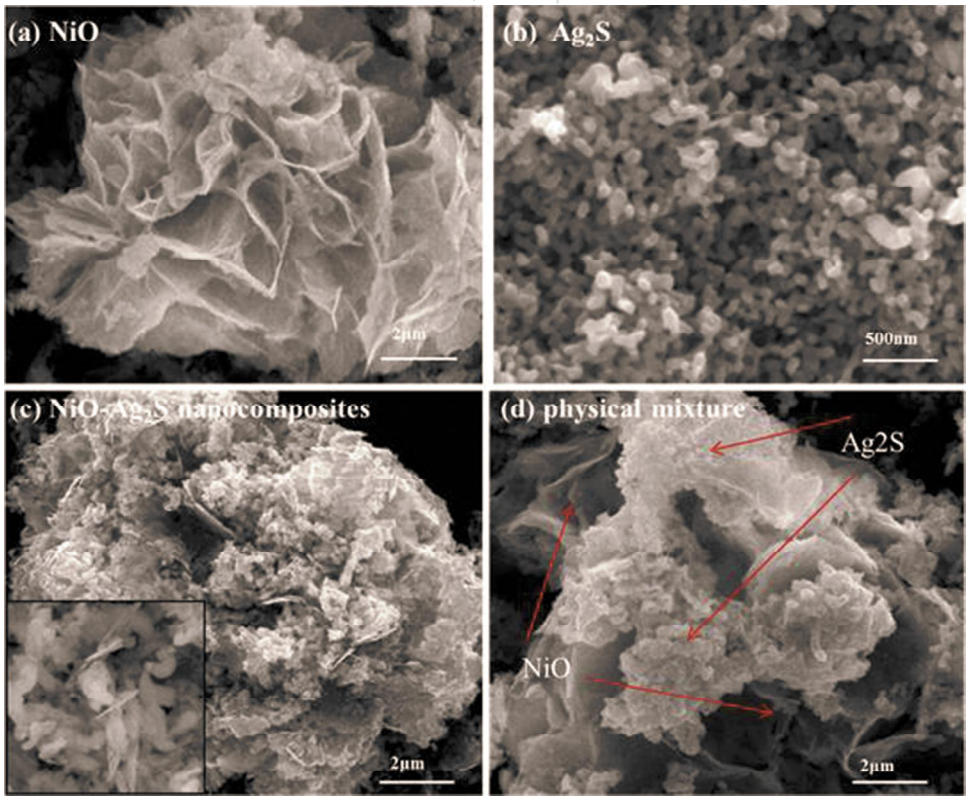

Fig. 1. SEM images of the morphology of (a) as-synthesized NiO; (b) Ag_2S nanoparticles; (c) NiO/Ag_2S nanocomposites and with an in for amplification view; (d) physical mixture.

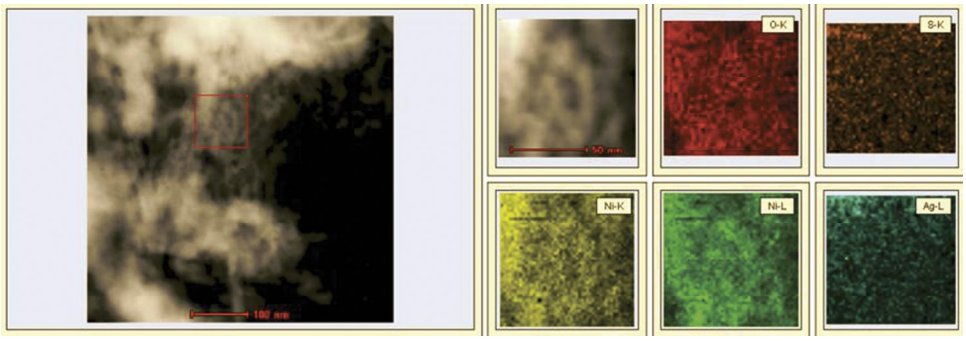

Fig. 2. Left: TEM photograph; Right: elemental mapping of NiO/Ag_2S nanocomposites.

and NiO/Ag_2S nanocomposite (mass ratio is 1:1) were observed by SEM, as shown in Figures 1(a)–(d), respectively. It can be seen that NiO displays a hollow flower shaped structure with some cross schistose petals, which have abundant spaces among the thin petals as shown in Figure 1(a). The Ag_2S nanoparticles shows elliptic spherical shape and the minimal axis and maximal axis of these nanoparticles are about 240 nm and 670 nm, respectively, as shown in Figure 1(b). In Figure 1(c), it can be observed that NiO/Ag_2S nanocomposites keep the similar flower shaped structure of as-synthesized NiO. However the spaces among these schistose petals are filled with Ag_2S nanoparticles which are uniformly and closely distributed in the schistose flower structures. By comparing with the products of hydrothermal process, the physical mixtures of NiO and Ag_2S are not mixed well, as shown in Figure 1(d). It is observed that the Ag_2S nanoparticles are agglomeration and not properly filled in hollow flower shaped structure of NiO. Obviously, hydrothermal process leads to more efficient mixing of NiO and Ag_2S. The uniformity of distribution of the NiO and Ag_2S nanocomposite is confirmed by a two-dimension EDX test. As shown in Figure 2, the colorful images indicates that the four elements (nickel, oxygen, silver and sulfide) uniformly distribute in NiO/Ag_2S nanocomposites. The results prove that the uniformly NiO/Ag_2S nanocomposites can be obtained by hydrothermal process.

From previous studies, the grain boundary of some metal oxides can be integrated during the growth of crystalline by hydrothermal method.[2] Comparison of XRD analyses allows us to well understand the binding features of grain boundaries between NiO/Ag_2S nanocomposites and the physical mixture of NiO and Ag_2S (the mass ratio of 1:1). As shown in Figure 3, the location of diffraction peaks of NiO/Ag_2S nanocomposites is almost the same to that of mixture of NiO and Ag_2S. The diffraction characteristic at 2θ of about 37.2°, 43.3°, 62.8°, 75.2°, and 79.4° due to the diffraction peaks of NiO phases, which can be indexed to the (111), (200), (220), (311), and (222) crystalline planes, respectively (JCPDS Card No. 4-0835). And the (111), (112), (121), (103), (031), (200), (213), and (134) crystal planes were indexed to the acanthite Ag_2S phase. The cell constants were calculated to be $a =$ 0.42261 nm, $b = 0.69$ nm, and $c = 0.78547$ nm (JCPDS 14-0072). By comparing with physical mixture of NiO and Ag_2S, the NiO/Ag_2S nanocomposite still maintained the diffraction peaks observed from NiO and Ag_2S. However, there are four diffraction peaks occurring at about 38°, 64.3°, 77.4° and 81.6°, respectively. It is noted that the diffraction peaks of NiO/Ag_2S nanocomposite have some shifts (about 0.15°) around 64°, 77° and 83° compared with physical mixture of NiO and Ag_2S. These results indicated that some bindings of the grain boundaries have generated in NiO/Ag_2S nanocomposites. Moreover, the relative intensity of diffraction peaks from the nanocomposite is very strong, while their width is narrow, compared to those from the physical mixture product, especially at high 2θ angles (from 50° to 90°). These observations reveal that the crystallinity of NiO/Ag_2S nanocomposite is better than that of the physical mixture product. Thus, we can conclude that the NiO/Ag_2S nanocomposite, which is showing good crystallinity, is different from the physical mixture.

The NiO/Ag_2S nanocomposites exhibit good visible light photocatalytic activity. For comparison, the visible light photocatalytic activity of Ag_2S nanoparticles, NiO flower shaped structures, physical mixture of NiO and

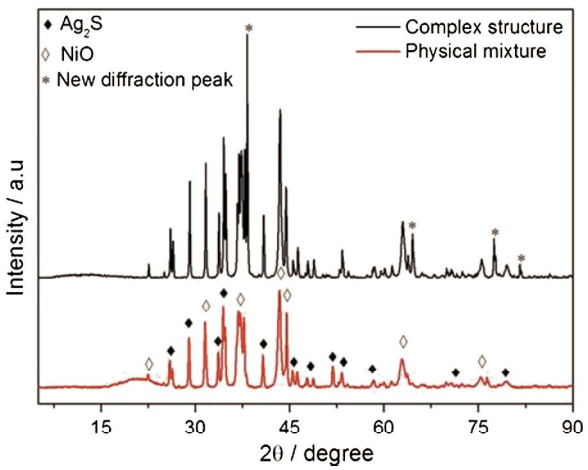

Fig. 3. XRD patterns of NiO/Ag_2S nanocomposites and phy ture of NiO and Ag_2S (the mass ratio of 1:1).

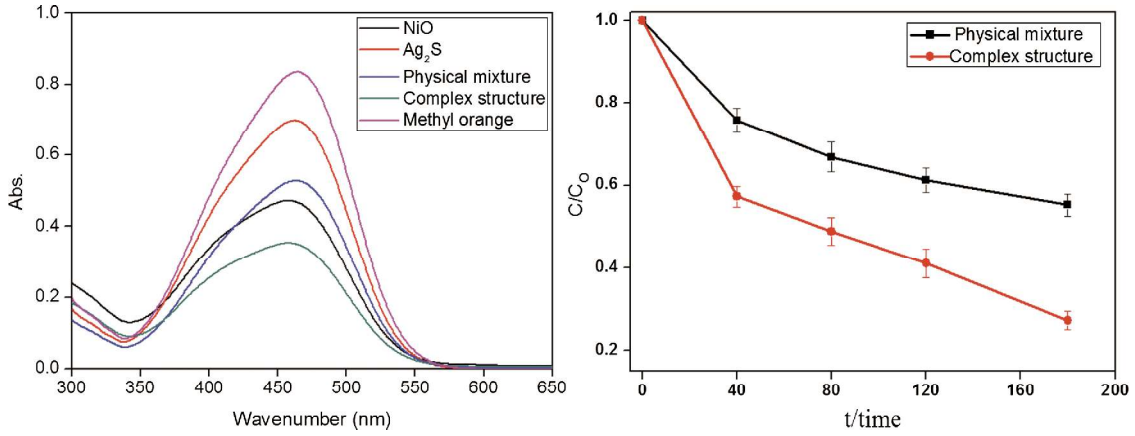

Fig. 4. (a) The UV-Vis adsorption spectra of the supernatant of NiO flower shaped structures, Ag_2S nanoparticles, the physical mixture of NiO and Ag_2S, and NiO/Ag_2S nanocomposites after illumination under Xe lamp for 120 min. (b) Degradation rates with error bars after different times for NiO/Ag_2S and physical mixture of nanocomposites NiO and Ag_2S.

Ag_2S are investigated under the same conditions. After illumination under Xe lamp for 120 min, the absorbance of the dye solution is shown in Figure 4(a). Obviously, among these four samples, NiO/Ag_2S nanocomposites have the highest photocatalytic activity. As we known, single NiO and Ag_2S have many disadvantages in photocatalytic activity, due to the bad light absorbance of the NiO and the serious agglomeration of Ag_2S nanoparticles. When the two materials simply mixed together, photocatalytic activity exhibit an averaging result as shown in Figure 4(a). In order to further investigate the photocatalytic activity of the NiO/Ag_2S nanocomposites, the MO degradation rates with error bar are also measured by spectrophotometer at 465 nm. As shown in Figure 4(b), the NiO/Ag_2S nanocomposites show better degradation rates than that of the physical mixtures of NiO and Ag_2S during 180 min. After illumination under Xe lamp for 180 min, the degradation rate of the NiO/Ag_2S nanocomposites increased to 60%, being 30% higher than that of the physical mixture. The good photocatalytic activity of NiO/Ag_2S nanocomposites can mainly be attributed to the larger contact areas (*p–n* junctions) of the two materials and the photo-generated electron–holes between the two materials. As shown in Figure 1(c), Ag_2S nanoparticles disperse uniformly in the flower shaped NiO framework which provides the efficient contact areas of the two materials. Furthermore, the contact between Ag_2S nanoparticles with the flower shaped NiO is not simply physical combine. The two materials have formed new grain boundaries and *p–n* junctions in the grain boundaries. Due to the charge collection capability of the *p–n* junctions, the photo-generated carriers can be easier to separate in the two materials. In the *p–n* junction, the accumulations of the electron and the hole reach the equilibrium, inducing the internal electric field, which can favorably prevent the electron–hole recombination. Because the electric field potential only allows the transfer of free electrons from the *p*- to *n*-type semiconductors and that of free holes from the *n*- to *p*-type semiconductors. It implies that the *p*-type semiconductor behaves as a hole-trapping species in this system. Thus, under the Xe lamp irradiation, the photo generated electron–hole pairs are efficiently separated, while their recombination is minimized and the successive photocatalytic degradation reactions stimulated by the freely moving electrons with prolonged lifetime are maximized. Therefore, the *p–n* junctions between NiO and Ag_2S could enhance the charge collection capability. Meanwhile, the higher crystalline of NiO/Ag_2S nanocomposites not only retain advantages of the single NiO_2 and Ag_2S materials, but prolongs the electron's lifetime in the nanocomposites.[9] Thus, NiO/Ag_2S nanocomposites exhibit the highest photocatalytic activity among these four samples.

4. CONCLUSIONS

In summary, the novel uniform NiO/Ag_2S nanocomposites are synthesized by hydrothermal process for the photocatalytic degradation under visible light irradiation. The flower shaped NiO/Ag_2S nanocomposites display 30% higher photocatalytic activity than that of physical mixtures after illumination under Xe light for 180 min. Through EDX and XRD analysis, the high photocatalytic properties of NiO/Ag_2S nanocomposite can be attributed to two points: the induced *p–n* junction at the interfacial contact between the NiO and Ag_2S phases and the uniform mixing of these two materials. This work offers novel NiO/Ag_2S nanocomposites which have great potential applications in photocatalysis.

Acknowledgment: This work is supported partially by National Natural Science Foundation of China (Grant nos. 91333122, 51402106, 51372082, 51172069, 50972032, 61204064 and 51202067), Ph.D. Programs Foundation of Ministry of Education of China (Gr 20110036110006, 20120036120006, 20130036

Par-Eu Scholars Program, and the Fundamental Research Funds for the Central Universities.

References and Notes

1. Y. Zhang, G. Hong, Y. Zhang, G. Chen, F. Li, H. Dai, and Q. Wang, *ACS Nano* 6, 3695 **(2012).**
2. F. Jiang, Q. Tian, M. Tang, Z. Chen, J. Yang, and J. Hu, *Cryst. Eng. Comm.* 13, 7189 **(2011).**
3. M. Pang, J. Hu, and H. C. Zeng, *JACS* 132, 10771 **(2010).**
4. W. L. Yang, L. Zhang, Y. Hu, Y. J. Zhong, H. B. Wu, and X. W. Lou, *Angew. Chem.* 124, 11669 **(2012).**
5. M. C. Neves, O. C. Monteiro, R. Hempelmann, A. M. S. Silva, and T. Trindade, *Eur. J. Inorg. Chem.* 28, 4380 **(2008).**
6. L. Zhu, Z.-D. Meng, and W.-C. Oh, *J. Nanomater.* 2012, 586526 **(2012).**
7. M. C. Neves, J. M. F. Nogueira, T. Trindade, M. H. Mendonça, M. I. Pereira, and O. C. Monteiro, *J. Photoch. Photobio. A* 204, 168 **(2009).**
8. Y. Xie, S. H. Heo, Y. N. Kim, S. H. Yoo, and S. O. Cho, *Nanotech.* 21, 015703 **(2010).**
9. Y. Ku, C.-N. Lin, and W.-M. Hou, *J. Mol. Catal. A-Chem.* 349, 20 **(2011).**
10. J. Yu, W. Wang, and B. Cheng, *Chem. Asian J.* 5, 2499 **(2010).**
11. S.-H. Lin, F.-R. Chen, and J.-J. Kai, *Appl. Surf. Sci.* 254, 3357 **(2008).**
12. X. Wang, J. Song, L. Gao, J. Jin, H. Zheng, and Z. Zhang, *Nanotech.* 16, 37 **(2005).**
13. H. Shu, J. Xie, H. Xu, H. Li, Z. Gu, G. Sun, and Y. Xu, *J. Alloy Compd.* 496, 633 **(2010).**
14. L. Ren, Y.-P. Zeng, and D. Jiang, *Solid State Sci.* 12, 138 **(2010).**
15. J. H. Kim, K. Zhu, Y. Yan, C. L. Perkins, and A. J. Frank, *Nano Lett.* 10, 4099 **(2010).**
16. H. Huang, S. X. Lu, W. K. Zhang, Y. P. Gan, C. T. Wang, L. Yu, and X. Y. Tao, *J. Phys. Chem. Solids* 70, 745 **(2009).**
17. T. Sreethawong, S. Ngamsinlapasathian, and S. Yoshikawa, *Chem. Eng. J.* 192, 292 **(2012).**
18. M. A. Ahmed, *J. Photoch. Photobio. A* 238, 63 **(2012).**
19. L. H. Chu, M. C. Li, P. Cui, Y. J. Jiang, Z. P. Wan, and S. Y. Dou, *Energy and Environment Focus* 3, 371 **(2014).**
20. L. H. Chu, M. C. Li, Z. P. Wan, L. Ding, D. D. Song, S. Y. Dou, J. W. Chen, and Y. Wang, *Cryst. Eng. Comm.* 16, 11096 **(2014).**

Received: 18 August 2014. Revised/Accepted: 4 March 2015.